frontiers | Frontiers in Earth Science

TYPE Original Research
PUBLISHED 18 January 2024
DOI 10.3389/feart.2023.1333668

OPEN ACCESS

EDITED BY
Yi Xue,
Xi'an University of Technology, China

REVIEWED BY
Subodh Chandra Pal,
University of Burdwan, India
Fei Liu,
Suzhou University, China

*CORRESPONDENCE
Jiangwei Zhang,
zjwok1988@sina.com
Xiaohui Cheng,
Chengxh@tsinghua.edu.cn

RECEIVED 05 November 2023
ACCEPTED 29 December 2023
PUBLISHED 18 January 2024

CITATION
Mao Q, Guo K, Zhang J, Xiao G, Du J, Cheng X and Guo H (2024), Response of granite residual soil slopes under dry–wet cycles.
Front. Earth Sci. 11:1333668.
doi: 10.3389/feart.2023.1333668

Response of granite residual soil slopes under dry–wet cycles

Qiang Mao[1], Kai Guo[1], Jiangwei Zhang[2,3]*, Guangning Xiao[3], Jianhang Du[2], Xiaohui Cheng[2]* and Hongxian Guo[2]

[1]Electric Power Research Institute, Ultra-High Voltage Transmission Company of China Southern Power Grid, Guangzhou, China, [2]Department of Civil Engineering, Tsinghua University, Beijing, China, [3]School of Urban Geology and Engineering, Hebei University of Geosciences, Shijiazhuang, China

Granite residual soil is widely distributed in the southern coastal areas of China, and the slopes of granite residual soil are prone to instability and failure under the alternating action of rainfall and drying, which will cause great disasters to human society. In order to study the response mechanism of granite residual soil slopes under the alternating action of rainfall–drying–static–rainfall (RDSR), this study conducted indoor scaling model tests to analyze the response during dry and wet cycles. This study presented the response process of the slope under the influence of dry and wet cycles and discussed the change laws of slope deformation, water content, and matric suction. The results show that, under the alternating action of rainfall–drying–static–rainfall, 1) the network cracks on the slope form a dominant channel for rainwater seepage, which is the main reason for the rapid decline in soil anti-sliding ability within a short time; 2) at a rainfall intensity of 1.7–2.4 mm/min, the erosion effect of rain on the slope is obviously stronger than that of osmotic erosion, and the surface erosion failure of the granite residual soil slope tends to occur without an obvious sliding surface; 3) after the loss of matric suction over a certain period, the phenomenon of channeling and loss failure on the slope serve as a sufficient condition for slope instability failure but is not a necessary condition. The above research results are expected to provide the basis and reference for preventing and controlling landslide hazards in granite residual soil slopes under similar conditions.

KEYWORDS

dry and wet cycles, granite residual soil, model test, matric suction, slope

1 Introduction

Granite residual soil is the detritus of granite that remains *in situ* after physical and chemical weathering. It is widely distributed in southern China, especially in southeastern coastal areas such as Guangdong and Fujian (Wu et al., 2004; Wu, 2006). Due to its special origin, granite residual soil has different engineering characteristics compared with common sedimentary soil in engineering and is prone to softening and disintegration when it encounters water (Wang et al., 1991; Zhang, 1994; Jian et al., 2003; Xu et al., 2017; Wang et al., 2023a; Wang et al., 2023b; Wang et al., 2023c; Wei et al., 2023). In the southeast coastal area, the climate is hot and humid, typhoons and rainstorms are frequent, and the temperature difference is large. This alternation between rainfall and drying increases the probability of a landslide event on granite residual soil slopes. This issue has also attracted the attention of relevant scholars. In order to study the water disintegration characteristics of granite residual soil, Zhang (2009) simplified the intergranular stress state of soil particles from a microscopic perspective and discussed the disintegration mechanism of unsaturated

granite residual soil, holding that the main controlling factors were pore pressure and matric suction inside the soil. Hu et al. (2015) studied the failure mode of granite residual soil slopes under rainfall through model tests, which were classified into four categories: deep integral failure, deep local failure, shallow integral failure, and shallow local failure. Meng et al. (2019) studied the rule of rainfall infiltration of granite residual soil slopes and believed that when rainwater infiltrated granite residual soil slopes, the infiltration route was roughly "flat parabola" and the moisture content of soil in the slope was roughly an inclined "L"-shape. Based on unsaturated seepage theory and unsaturated soil mechanics theory, Zhang (2017) and Yang (2019) discussed the influence laws of rainfall conditions, slope morphology, physical and mechanical parameters on slope seepage fields, and stability through test and numerical simulation methods. In terms of research methods, direct shear tests, laboratory tests, physical model tests, and numerical analyses have been widely used and achieved good results (Xu, 2015; Liu et al., 2021; Yao, 2021; YANG et al., 2022).

The soil–water characteristic curve is a key issue in the stability analysis of edge slope rainfall, and scholars have extensively researched this topic (Satyanaga et al., 2013; Alves et al., 2020; Hedayati et al., 2020). Kristo et al. (2019) applied the combination of soil–water characteristic curves considering dry and wet conditions to the safety factor of slopes. Based on the VG model, Ma et al. (2021) proposed a prediction model that considered both matric suction and dry and wet cycles, and the fitting results of Nanning expansive soil and volcanic ash soil were good.

Furthermore, landslide susceptibility prediction based on a semi-supervised multiple-layer perceptron model has been studied, and the fully connected sparse autoencoder (FC-SAE) is

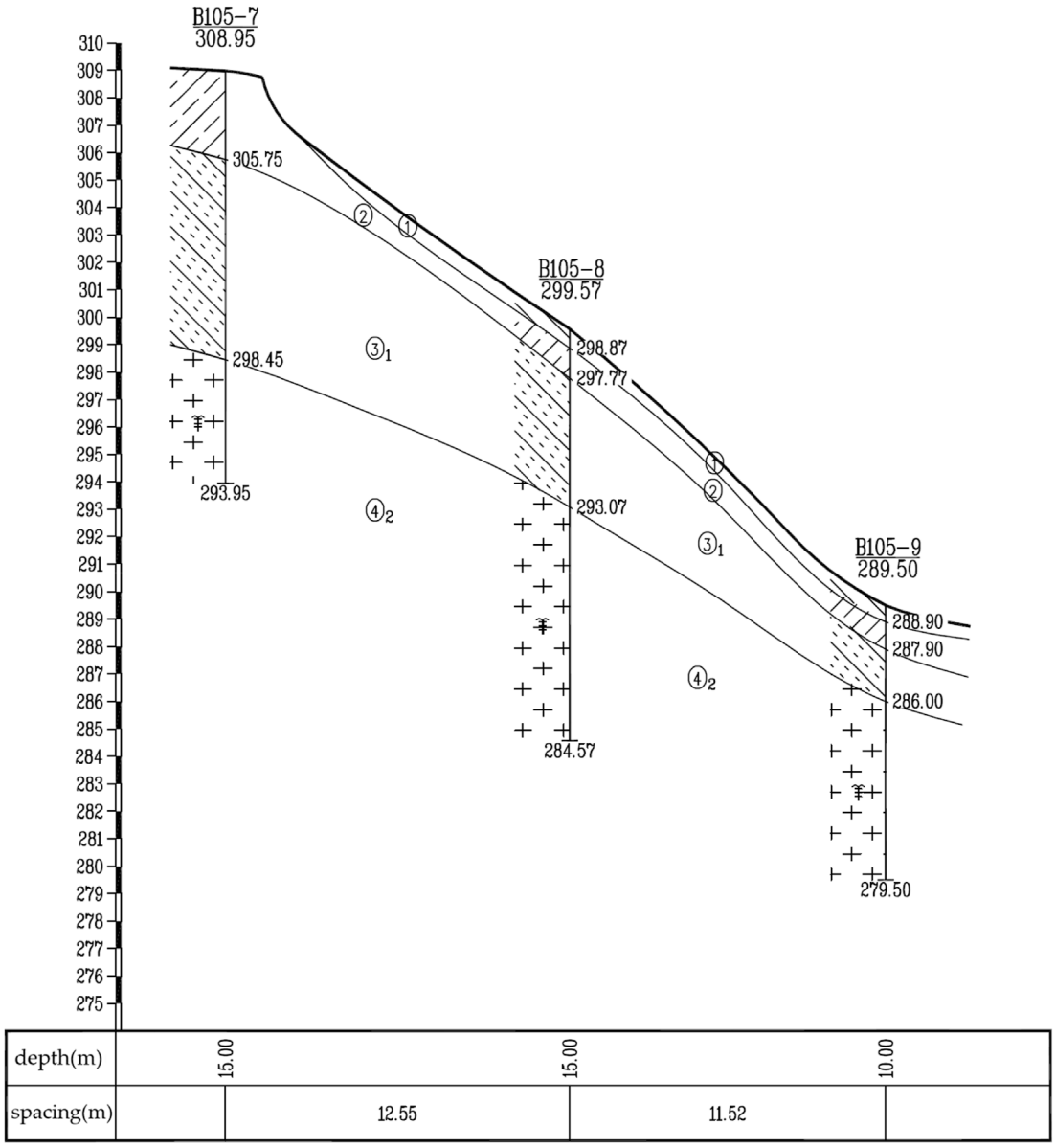

FIGURE 1
Engineering geological profile.

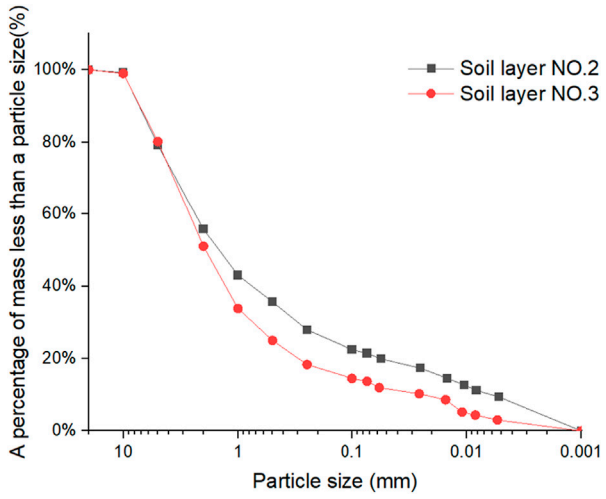

FIGURE 2
Soil size distribution curve.

proposed for landslide susceptibility prediction (Jiang et al., 2018; Huang et al., 2020a; Huang et al., 2020b; Chang et al., 2020; Huang et al., 2020c; Zhang et al., 2022). Based on the Green–Ampt model, Pan et al. (2020) comprehensively considered the initial water content, groundwater level, and unsaturated characteristics of the slope and established an infiltration model suitable for different rainfall conditions.

In conclusion, several studies have been carried out on the response and stability of granite residual slopes under rainfall, and good results have been obtained. The focus of this paper is to study the response of granite residual soil slopes under the load condition of a multi-type cycle of rainfall–drying–static–rainfall (RDSR), considering the influence of rainfall intensity. Taking the granite residual soil in the Guangdong area as the research object, the method of laboratory-scale model testing is adopted. The response law of slopes under the multi-type cycle of RDSR is studied fundamentally by the change laws of slope deformation, water content, and matric suction in order to provide a basis for preventing and controlling the major landslide disasters on granite residual soil slopes under the action of multiple types.

2 Model test

2.1 Model soil

The model built in this paper takes a slope in Qingyuan, Guangdong Province, as an example, and its engineering geological profile is shown in Figure 1. The slope is 32°–38°, and the slope height is approximately 40 m. According to the on-site geological survey and drilling, the quaternary overlying strata in the landslide area mainly include landslide-accumulated soil caused by slump accumulation, silty clay caused by slope accumulation, and sandy, viscous soil caused by residual accumulation, and the underlying bedrock is Yanshan granite. The specific characteristics are described below.

The first layer, identified as landslide accumulation soil (①$_1$), appears brown-yellow and grayish-yellow. It is slightly wet and loose, mainly composed of residual viscous soil and weathered rock, resulting from upper slope sliding or collapse. This layer is mixed

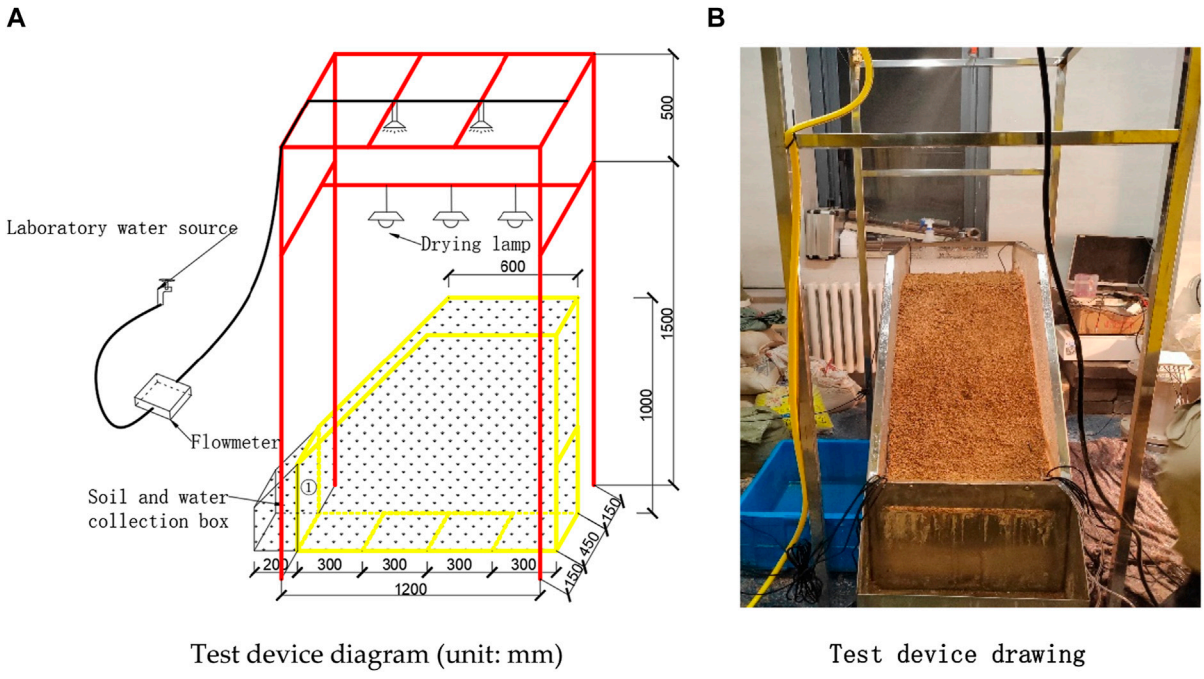

FIGURE 3
Soil size distribution curve. **(A)** Test device diagram (unit: mm). **(B)** Test device drawing.

with a large amount of strongly weathered rock and plant roots, presenting a disorderly and loose structure, attributed to the cause of collapse accumulation. This layer is mainly distributed in the surface layer of the middle and downhill sections, where shallow surface landslides occur, and the exposed thickness is 1.40–1.70 m. The second layer, identified as silty clay (②), appears brown-yellow and grayish-yellow. It is wet, plastic and contains a large amount of medium-coarse sand particles. The viscosity is general, and local water easily softens this layer, contributing to slope formation. This layer is distributed throughout the whole hillside but is generally absent in the upper and middle parts of the landslide area, with an exposed thickness of 1.50–3.60 m. The third layer, identified as sandy, viscous soil ($③_1$), appears yellow-brown and grayish-brown. It is slightly wet, hard plastic, with poor viscosity and a rough section. It contains a large number of quartz, coarse-sand, and gravel sand particles, displaying a local residual original rock structure. It is easy to disperse by hand and easily softens upon contact with water, contributing to residual deposition. This layer is distributed across the whole slope; the exposed thickness is 2.40–2.90 m, and further down is the bedrock layer.

The finite element numerical simulation method uses the actual ground motion input to truly reflect the dynamic response characteristics of the slope under the earthquake action and is not limited by the geologic conditions, geometric configuration, or other factors of the slope, which can solve the problem that is difficult to solve using the analytical method and more realistically and reasonably evaluate the dynamic stability of the slope under the earthquake action when studying and analyzing the slope stability under the earthquake action. Therefore, the finite element numerical simulation method is widely and deeply applied in solving the seismic stability problem of slopes.

In order to study the particle size characteristics of the granite residual soil, the second and third layers of soil were retrieved from the site for experimental study, and the soil was naturally air-dried for particle analysis tests. The particle size gradation curves are shown in Figure 2. The d50 of soil layer No. 2 is 1.48 mm, and the d50 of soil layer No. 3 is 1.92 mm. The grain size distribution is characterized by a high content of coarse particles, a similar content of gravel and sand, and a low content of fine particles. According to the engineering classification standard of soil GB-T50145-2007, soil layers No. 2 and No. 3 are named silty sand and grained sand, respectively.

2.2 Scale model of slopes

The size of the model box is length × width × height (rear edge) =1.2 m × 0.45 m × 1 m. Transparent plexiglass is installed on both sides and the back wall of the model box, and soil and water collection boxes are installed at the front end. The dry and wet circulation system is composed of a laboratory water source, water pipe, rainfall nozzle, and high-power drying lamp, and the rainfall height is 2 m, as shown in Figure 3.

Based on the actual slope proportion and pre-test results, the soil slope is simplified into two layers corresponding to the second and third layers of soil mentioned above in order to better understand the response problem under the dry–wet cycle, as shown in Figure 4. The lower layer is the ③ soil layer, the upper layer is the ② soil layer, the dry density is 1.41 g/cm^3, and the water content is 16.9%. The slope model of granite residual soil is constructed by artificial layer-by-layer filling with a distance of 5 cm between each layer. Matric suction and moisture content sensors are installed at the top of the slope, the midpoint of the slope bottom, and the three points of the slope and numbered successively to monitor the response of matric suction and moisture content along the surface and depth of the slope. The sensor layout diagram is shown in Figure 4. The sensor used is shown in Figure 5. The moisture content sensor used in this study is EC-5, obtained from Washington, United States, and the matric suction sensor used in this study is TEROS 21, which is obtained also from Washington, United States.

2.3 RDSR

The simulated test rainwater is laboratory tap water, and the flow rate is controlled using a flowmeter and water valve to realize the simulation of different rainfall intensities. The calibration is made according to the standard T/CMSA 0013 2019 (China Meteorological Service Association, 2019) for short-time meteorological service rainfall levels, and the short-time heavy rainstorm level is reached by controlling the flowmeter control water valve. In order to achieve as much as possible the situation of natural rain, the nozzle can simulate the state of natural raindrops. The simulation test sunshine is to dry the slope after rain through a high-power lamp and maintain the surface temperature of the slope at 40°C–50°C. The dry and wet cycle conditions are listed in Table 1. The test procedure is as follows:

TABLE 1 Dry and wet load conditions.

Time	RDSR
48 min	Rainfall intensity (2.4 mm/min)
12 h	Dry
11 h	Static
48 min	Rainfall intensity (1.7 mm/min)

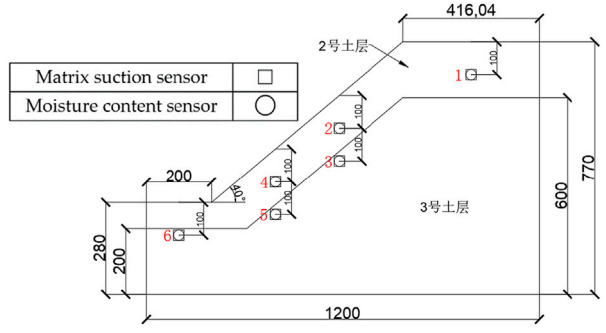

FIGURE 4
Sensor layout position (unit: mm).

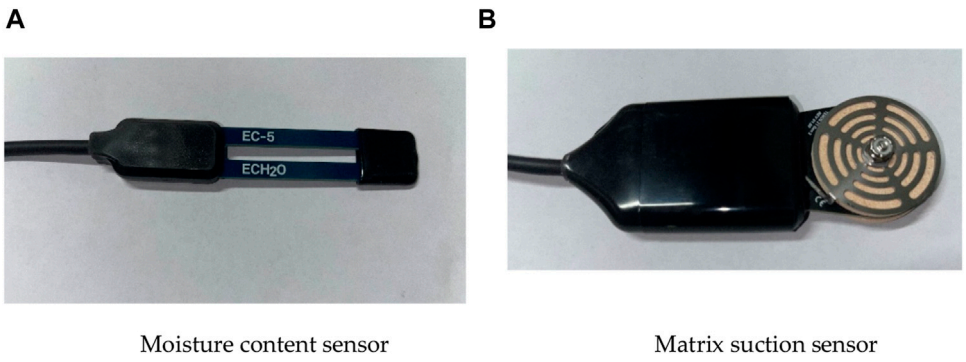

FIGURE 5
Sensor type. **(A)** Moisture content sensor. **(B)** Matric suction sensor.

3 Test results and analysis

3.1 Deformation rule

After the dry and wet alternating action of rainfall–drying–static–rainfall, the slope model presents different deformation laws. Figure 6 shows the slope deformation under different conditions. As can be seen from the figure, during 48 min of the first rainfall, part of the rainwater penetrated into the slope, and part of it ran off along the slope to the foot of the slope and carried away the surface soil of the slope. Due to the erosion of the slope shoulder, local shallow water holes appeared and spread along the slope foot, and then erosion damage and disintegration damage occurred simultaneously in a small local area of the slope. The scour range of the largest place is reached, the width of the shallow sinkhole is 4 cm, and the length is 6 cm. After drying and static for 23 h, the moisture content of the soil on the slope decreases and the color becomes lighter, but no cracks appear. According to the above particle size grading curve of the soil, d50 = 1.48 mm, the soil belongs to sandy soil, the soil viscosity is low, and the shape of the sand gravel is more obvious and prominent after drying. After 48 min of continuous rainfall, the sinkhole caused by the first rainfall became shallower, which was caused by the filling of the soil in the upper reaches after the rainfall erosion. Meanwhile, the surrounding soil was carried away by the rain, which led to the expansion of the damage ranging from 4 to 7 cm in width and from 6 to 11 cm in length. A relatively large range of erosion and damage occurred in the upper reaches, forming a depression. The rainwater carries mud and sand runoff and erodes to form several radial gullies downstream, and the washed mud and sand accumulate at the foot of the slope. The deposits at the broken corners after the first rainfall and the second rainfall were taken, and it was found that the rainfall after drying resulted in more soil and water loss, as shown in the figure. It can be seen that after drying, the surface layer of the soil becomes looser, micro-cracks appear, and advantageous

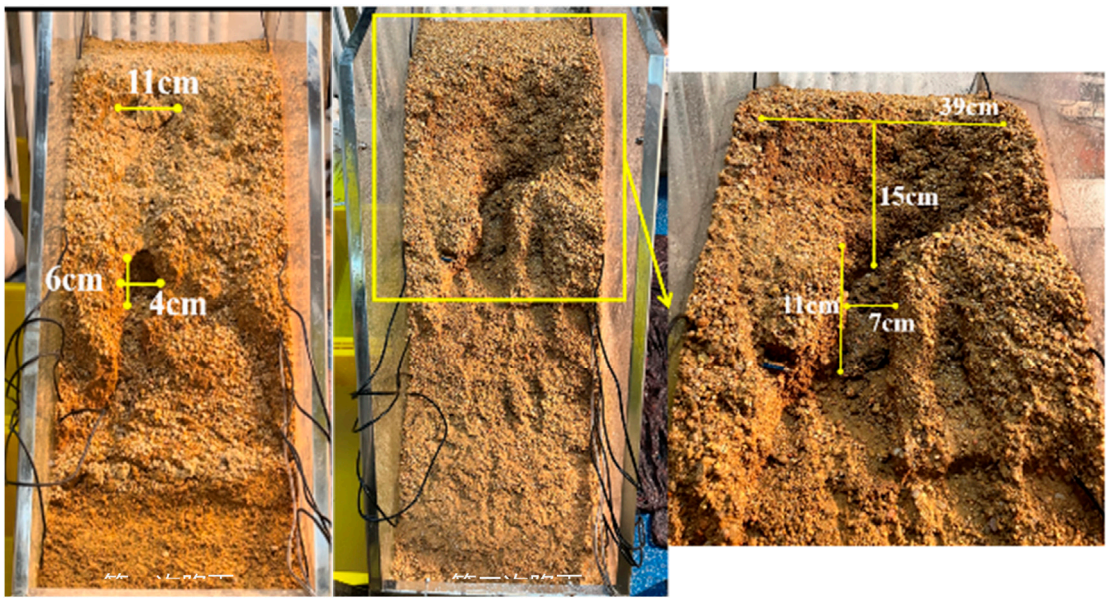

FIGURE 6
Slope deformation characteristics under dry and wet cycles.

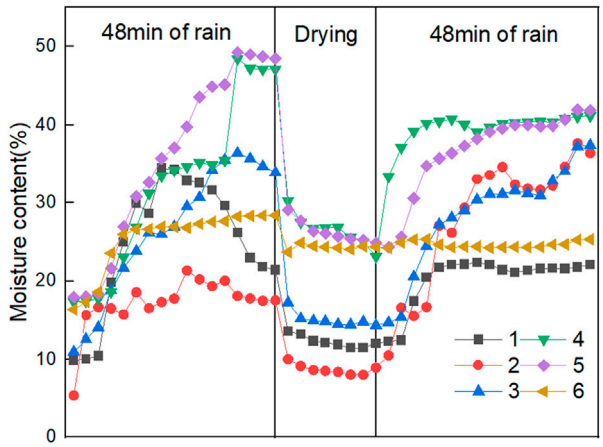

FIGURE 7
Water ratio curve of the targets.

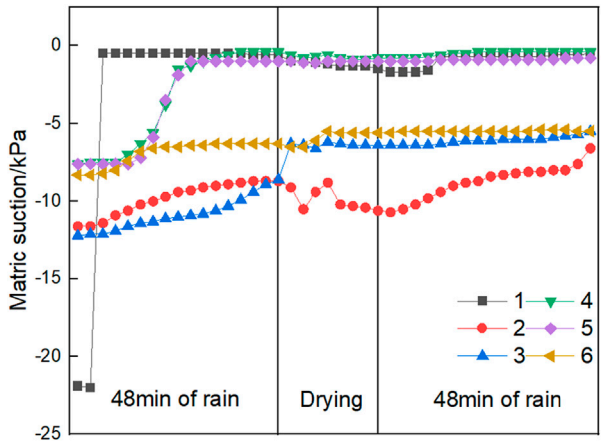

FIGURE 8
Matric suction curve of the targets.

channels of seepage are formed. The same rainfall duration and intensity lead to rapid water absorption and softening of the soil, resulting in more soil and water loss.

3.2 Law of moisture content change

Figure 7 shows the change curve of water content at each monitoring point during the dry-wet cycle. Before rainfall, the volume moisture content of each monitoring point was 15% on average, and point 2 on the slope may have been low due to the error caused by uneven model making. With the progress of rainfall, the moisture content of each monitoring point increased rapidly and reached its highest point in approximately 30 min. Among them, the moisture content of monitoring points No. 4 and No. 5 at the foot of the slope also rose the fastest, reaching approximately 48% after 48 min of rainfall. After drying and static for 23 h, the overall moisture content decreased, and the moisture content at the No. 2 and No. 3 points near the slope shoulder decreased the most, even approaching the pre-rainfall level. After 48 min of rainfall, the moisture content of each point showed an overall upward trend. Due to the formation of a stable infiltration channel, it soon reached a relatively stable state, and the overall moisture content was lower than the level of the first rainfall. On the whole, the moisture content at the No. 4 and No. 5 points at the foot of the slope has the most significant growth rate and maximum value during the rainfall process, which confirms the position of the above rainwater flushing channel. This may be due to the fact that the foot of the slope is at the intersection of seepage, and according to the deformation of the slope surface, the gully caused by rainfall erosion is located just below the slope surface, causing the thickness of the soil above the sensor to become thinner, thereby accelerating the infiltration rate of rainwater. Meanwhile, the superposition of rainfall on the surface and internal seepage of the slope surface lead to a significant increase in the moisture content of the area.

3.3 Variation in matric suction

The variation in matric suction is consistent with that in the water content on the whole. This is due to the increase in the water content, which fills the pores of the soil and makes the matric suction gradually decrease, which shows an upward trend and tends to 0, as shown in the Figure 8. In the process of the first rainfall, with the increase in the water content in all parts of the slope, the matric suction at all points decreased, and the matric suction at points No. 4 and No. 5 at the foot of the slope had the largest decrease. After approximately 30 min of rainfall, the matric suction at point No. 5 was close to 0. The interaction between the water content and matric suction is also confirmed. This also corresponds to the local erosion failure of the surface of the slope. After drying, the matric suction at all points shows a rebound phenomenon on the whole, but the amplitude is small. It can be seen that the drying–static process has no great influence on the water content and matric suction at the deep part of the slope, and the matric suction at the surface at the top and shoulder of the slope has the largest rebound. It can be seen that drying reduces the water content of the surface soil and then causes the matric suction to increase, showing a downward trend in the figure. In the second rainfall, the matric suction at the No. 2 and No. 3 points on the slope shoulder continued to decrease, and the matric suction at the other points basically stabilized. It can be seen that in this slope model, water content and matric suction basically reach their peak state after 48 min of rainfall.

4 Conclusion

Through laboratory model tests and numerical simulation methods, the response of granite residual soil slopes to deformation, moisture content, and matric suction under the multi-type cycle of RDSR conditions was studied. Based on the numerical examples in this study, the following conclusions were obtained:

(1) The drying and static effects after rainfall lead to the rapid appearance of network cracks on the slope, with a width of approximately 1 mm and a depth of approximately 10–30 mm, which promotes the formation of a dominant seepage channel

on the slope, resulting in a rapid decline in soil resistance to sliding under relatively small rainfall intensity (the rainfall intensity before drying load is 2.4 mm/min and the rainfall intensity after drying is 1.7 mm/min) and an increase in the amount and speed of topsoil washed away by rain.

(2) Under a rainfall intensity of 2.4 mm/min, the slope of granitic residual soil with large coarse-grained components tends to have surface erosion and failure, and there is no obvious sliding surface. Under the cyclic alternating action of superimposed drying, static, and rainfall, the slope surface is more susceptible to instability, such as local gullies and shallow fall holes. Particularly after drying, the surface of the soil becomes even looser, exhibiting network cracks and forming a seepage channel, which leads to more soil and water loss.

(3) During rainfall, the changes in water content and matric suction show consistency. The mechanical mechanism of slope instability failure is that the increase in the water content leads to the decline in matric suction, and then the anti-sliding ability of soil decreases until the limit equilibrium is broken and landslide failure occurs. However, from this study, the loss of matric suction is more of a sufficient condition for slope instability than a necessary condition.

It can be seen that the protection of granite residual soil slopes is particularly important, especially in the rainy areas in the south. Protective measures can focus on strengthening the protection of the slope, including the use of slope protection, biological reinforcement, and other ecological and low-carbon measures. The purpose of protection is first to solidify the slope surface and reduce water and soil loss caused by rain erosion and second to prevent the slope instability caused by rain infiltration.

It is worth noting that the research results are only carried out under the condition of this model without considering the influence of geometry and model size. Conducting further centrifuge model tests that consider model size can obtain more scientifically valid and reasonable research results.

Data availability statement

The original contributions presented in the study are included in the article/Supplementary Material; further inquiries can be directed to the corresponding authors.

Author contributions

QM: funding acquisition, resources, and writing–review and editing. KG: funding acquisition, resources, and writing–review and editing. JZ: conceptualization, data curation, and writing–review and editing. GX: writing–review and editing. JD: writing–review and editing. XC: conceptualization, investigation, and writing–review and editing. HG: formal analysis, investigation, and writing–review and editing.

Funding

The author(s) declare financial support was received for the research, authorship, and/or publication of this article.

Acknowledgments

The authors are grateful to the Electric Power Research Institute, Ultra-High Voltage Transmission Company of China Southern Power Grid, for providing research funding. All statements, results, and conclusions are those of the researchers and do not necessarily reflect the views of these foundations. The authors would also like to sincerely thank the reviewers for their insightful comments and suggestions.

Conflict of interest

Authors QM and KG were employed by Ultra-High Voltage Transmission Company of China Southern Power Grid.

The remaining authors declare that the research was conducted in the absence of any commercial or financial relationships that could be construed as a potential conflict of interest.

Publisher's note

References

Alves, R. D., Gitirana, G. D., and Vanapalli, S. K. (2020). Advances in the modeling of the soil-water characteristic curve using pore-scale analysis. *Comput. Geotechnics* 127, 1–12. doi:10.1016/j.compgeo.2020.103766

Chang, Z., Du, Z., Zhang, F., Huang, F., Chen, J., Li, W., et al. (2020). Landslide susceptibility prediction based on remote sensing images and GIS: comparisons of supervised and unsupervised machine learning models. *Remote Sens.* 12, 502. doi:10.3390/rs12030502

China Meteorological Service Association (2019). *The grade of rainfall in short time weather service T/CMSA 0013 2019.*

Hedayati, M., Ahmed, A., Hossain, M., Hossain, J., and Sapkota, A. (2020). Evaluation and comparison of *in-situ* soil water characteristics curve with laboratory SWCC curve. *Transp. Geotech.* 23 (0), 100351–100412. doi:10.1016/j.trgeo.2020.100351

Hu, H., Cai, L., Liang, J. Y., and Li, X. (2015). Experimental research on impact damage and damage evolution characteristics of granitic saprolite. *Rock Soil Mech.* 36 (S1), 25–30. doi:10.16285/j.rsm.2015.S1.005

Huang, F., Cao, Z., Guo, J., Jiang, S.-H., Guo, Z., and Guo, Z. (2020a). Comparisons of heuristic, general statistical and machine learning models for landslide susceptibility prediction and mapping. *CATENA* 191, 104580. doi:10.1016/j.catena.2020.104580

Huang, F., Cao, Z., Jiang, S.-H, Zhou, C., Guo, Z., and Guo, Z. (2020c). Landslide susceptibility prediction based on a semi-supervised multiple-layer perceptron model. *Landslides* 17, 2919–2930. doi:10.1007/s10346-020-01473-9

Huang, F., Zhang, J., Zhou, C., Wang, Y., Huang, J., and Zhu, L (2020b). A deep learning algorithm using a fully connected sparse autoencoder neural network for landslide susceptibility prediction. *Landslides* 17 (01), 217–229. doi:10.1007/s10346-019-01274-9

Jian, W. B., Chen, W. Q., and Zheng, D. X. (2003). "Experimental study on disintegration of granite residual soil China civil engineering society," in *Proceedings of the 9th academic conference on soil mechanics and geotechnical engineering of the Chinese society of civil engineering (Part 1)* (Beijing, China: Tsinghua University Press), 312–315.

Jiang, S. H., Huang, J., Huang, F., Yang, J., Yao, C., and Zhou, C. (2018). Modelling of spatial variability of soil undrained shear strength by conditional random fields for slope reliability analysis. *Appl. Math. Model.* 63, 374–389. doi:10.1016/j.apm.2018.06.030

Kristo, C., Rahardjo, H., and Satyanaga, A. (2019). Effect of hysteresis on the stability of residual soil slope. *Int. Res. Soil Water Conservation* 7 (3), 226–238. doi:10.1016/j.iswcr.2019.05.003

Liu, Y., Chen, D. X., Wang, H., and Yu, J. J. (2021). Response analysis of residual soil slope considering crack development under drying-wetting cycles. *Rock Soil Mech.* 42 (07), 1933–1943. doi:10.16285/j.rsm.2020.1504

Ma, S., Huang, X., Duan, Z., Ma, M., and Shao, Y. (2021). New prediction model for SWCC of expansive soil considering drying and wetting cycles. *J. Mt. Sci.* 57 (3), 393–404. doi:10.1134/s1062739121030054

Meng, Q. S., Huang, Q. S., and Lan, S. L. (2019). Experimental study on rainfall infiltration of granite residual soil slope. *West. China Commun. Sci. Technol.* (6), 4.

Pan, Y. L., Jian, W. X., Li, L. J., Lin, Y. Q., and Tian, P. F. (2020). A study on the rainfall infiltration of granite residual soil slope with an improved Green-Ampt model. *Rock Soil Mech*. doi:10.16285/j.rsm.2019.1734

Satyanaga, A., Rahardjo, H., Leong, E. C., and Wang, J. Y. (2013). Water characteristic curve of soil with bimodal grain-sizedistribution. *Comput. Geotechnics* 48, 51–61. doi:10.1016/j.compgeo.2012.09.008

Wang, L., Xue, Y., Cao, Z., Kong, H., Han, J., and Zhang, Z. (2023a). Experimental study on mode I fracture characteristics of granite after low temperature cooling with liquid nitrogen. *Water* 15, 3442. doi:10.3390/w15193442

Wang, L., Xue, Y., Cao, Z., Wu, X. J., Dang, F. N., and Liu, R. (2023c). Mechanical properties of high-temperature granite under liquid nitrogen cooling. *Geofluids* 2023, 1–23. doi:10.1155/2023/3819799

Wang, L., Zhang, W., Cao, Z., Xue, Y., Liu, J., Zhou, Y., et al. (2023b). Effect of weakening characteristics of mechanical properties of granite under the action of liquid nitrogen. *Front. Ecol. Evol.* 11, 1249617. doi:10.3389/fevo.2023.1249617

Wang, Q., Tang, D. X., and Zhang, Q. Y. (1991). Study on composition and structural characteristics of granite residual soils in eastern China. *J. Jilin Univ. Sci. Ed.* 21 (1), 75–83.

Wei, L., Dang, F., Ding, J., Wu, X., Li, J., and Cao, Z. (2023). An analysis of thixotropic micropore variation and its mechanism in loess. *Front. Ecol. Evol.* 11, 1242462. doi:10.3389/fevo.2023.1242462

Wu, N. S. (2006). Study on classification of granite residual soils. *Rock Soil Mech.* 27 (12), 2299–2304.

Wu, N. S., Zhao, C., and Hou, W. S. (2004). Research on the cause of formation, distribution and engineering characteristics of the granite residual soil. *J. Pingdingshan Inst. Technol.* (04), 1–4.

Xu, X. T. (2015). *Research on the response and failing process of unsaturated residual soil slope under rainfall infiltration*. Fuzhou, China: Fuzhou University.

Xu, X. T., Jian, W. B., and Wu, N. S. (2017). Influence of repeated wetting cycles on shear properties of natural residual soil. *China J. Highw. Transp.* 30 (2), 33–40.

Yang, X. (2019). *Analysis of seepage and stability of meizhou granite residual soil slope under rainfall conditions*. Guangzhou, China: South China University of Technology.

Yang, X. F., Chen, D. X., and Liu, Y. (2022). Crack development and slope stability of granite residual soil under dry-wet cycles. *J. Xiamen Univ. Nat.* 61 (04), 591–599.

Yao, X. R. (2021). *Research on fluid-solid coupling analysis of granite residual soil slope stability*. Hengyang, China: University of south china.

Zhang, J. W., Chen, S., Wang, T. Y., and Wu, F. B. (2022). Study on correlation between ground motion parameters and soil slope seismic response. *Bull. Eng. Geol. Environ.* 81, 226. doi:10.1007/s10064-022-02725-9

Zhang, S. B. (2017). Stability analysis on unsaturated granite residual soil slope under the rainfall action. *Fujian Archit. Constr.* (12), 5.

Zhang, W. H. (1994). Analysis of shear strength and soil slope stability of granite residual soil. *Hydrogeology Eng. Geol.* (3), 41–43.

Zhang, Z. (2009). *Study on disintegration behavior of granite residual soil in guangzhou*. Wuhan, China: China University of Geosciences.